International Journal of Pharmaceutics: X 8 (2024) 100304

Contents lists available at ScienceDirect

International Journal of Pharmaceutics: X

journal homepage: www.sciencedirect.com/journal/international-journal-of-pharmaceutics-x

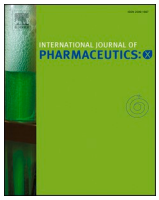

Mechanistic insights of desmopressin loaded elastic liposomes for transdermal delivery: HSPiP predictive parameters and instrumental based evidences

Afzal Hussain [a,*], Mohammad A. Altamimi [a,*], Musaad A. Alshammari [b]

[a] Department of Pharmaceutics, College of Pharmacy, King Saud University, Riyadh 11451, Saudi Arabia
[b] Department of Pharmacology, College of Pharmacy, King Saud University, Riyadh 11451, Saudi Arabia

ARTICLE INFO

Keywords:
Hansen solubility parameters
Elastic liposomes
Desmopressin acetate
Transdermal permeation
Microscopic skin visualization

ABSTRACT

Desmopressin acetate (DA) is a first-line option for the treatment of hemophilia A, von Willebrand's disease, nocturnal enuresis, central diabetes insipidus, and various traumatic injuries. We extended previously reported desmopressin-loaded elastic liposomes (ODEL1) to investigate mechanistic insights into ODEL1 mediated augmented permeation across rat skin. HSPiP software and instrumental techniques such as differential scanning calorimeter (DSC), Fourier Transform infrared (FTIR), scanning electron microscopy (SEM), and fluorescent microscopy provided better understandings of permeation behavior. HSPiP was used to compare Hansen solubility parameter (HSP) of ODEL1, DA, components, and rat skins (control and treated) in terms of dispersion forces (δ_d), polar forces (δ_p), and hydrogen bonding (δ_h). FTIR, DSC, fluorescence microscopy, and SEM provided a detailed mechanistic understanding of the changes occurred after treatment. The values of δ_d, δ_p, and δ_H for DA were 20.6, 31.9, and 18.2 $MPa^{1/2}$, respectively, whereas these were 15.6, 14.97, and 2.4 $MPa^{1/2}$ for ODEL1, respectively, suggesting remarkable permeation of DA by changing innate cohesive energies of the skin. DA primarily interacts through δ_d and δ_p with the ODEL1 and the skin. Furthermore, the stretching and bending vibrations (molecular interactions) of the treated skins were quite diverse as compared to the untreated skin. ODEL1 caused a substantial thermal changes (shifted 67 to 65 °C, and 79 to 82.5 °C) for the surface protein and glycoprotein as compared to the untreated skin. Fluorescence and SEM confirmed relatively intense surface perturbation of the treated skin as compared to the control. Thus, ODEL1 was efficient in interacting with the skin surface for reversible changes and subsequently resulted in high permeation and drug deposition.

1. Introduction

Desmopressin acetate (DA) treats hemophilia A, von Willebrand's disease, nocturnal enuresis, central diabetes insipidus, and various traumatic injuries. DA is delivered through various routes due to high hepatic and enzymatic degradation (in the gut and nasal passages). The doses in dosage forms are determined based on the routes of administration (parenteral delivery of 20–40 μg, oral dose of 100–200 μg, nasal dose of 20–40 μg). Oral and nasal routes resulted in limited bioavailability (BA) such as < 1 % and 3.4 %, respectively (Dirscherl et al., 2010; Lin et al., 2008). Peptide based DA is sensitive to α-chymotrypsin, leading to inactivation (Kyounghee et al., 2018; Wu et al., 2018). Cormier et al. employed an expensive, laborious, and patient unfriendly microneedle array (Macroflux®) method to deliver DA to achieve 85 % (± 30) BA by modulating SC (*stratum corneum*) layer (Alkilani et al., 2015; Cormier et al., 2004). Therefore, transdermal route of drug delivery is the most preferred route of delivery due to several advantages, including multiple dose adjustment, ease of application, avoidance of hepatic metabolism, minimal adverse effects, and high patient compliance. The route maintains the plasma drug concentration in wider range of absorption due to slow and sustained drug permeation across the skin. Moreover, oral delivery of desmopressin acetate is associated with the dryness of mouth and headache. Therefore, it was anticipated to mitigate the drug associated side effects after transdermal delivery.

To sustain the drug delivery, the vesicular elastic liposomes and transdermal administration were chosen based on the suitability of DA and its pharmaceutical properties (high pKa as 12, low dose, an isoelectronic point of 10.22, gut sensitivity, variable bioavailability,

* Corresponding authors.
E-mail addresses: amohammed2@ksu.edu.sa (A. Hussain), maltamimi@ksu.edu.sa (M.A. Altamimi).

https://doi.org/10.1016/j.ijpx.2024.100304
Received 20 May 2024; Received in revised form 6 November 2024; Accepted 10 November 2024
Available online 13 November 2024

short elimination half-life, high stability in liposomes as 177 h, at pH 4, and low aqueous solubility) (Altamimi et al., 2021a; Cormier et al., 2004; Hussain et al., 2016). Elastic liposomes are biocompatible, cholesterol free, and economic vesicular system for transdermal delivery. Elastic liposomes are quite ultra-deformable and flexible as compared to conventional liposomes (containing cholesterol) for dermal access. This may augment permeation and effective treatment for nocturnal enuresis. In our previous report, QbD (quality by design) oriented ODEL1 (optimized desmopressin loaded elastic liposomes) was associated with low vesicle size (119 nm), high entrapment (79 %), and enhanced permeation flux (7.5 μg/h·cm^2) across rat skin (Altamimi et al., 2021a). We followed up the work and aimed to encourage mechanistic understanding of vesicular permeation and interaction of ODEL1 and ODEL2 (the second optimized elastic liposomes), as compared to DS (drug solution) using HSPiP program and instrumental tools (Altamimi et al., 2021a). A detailed information of desmopressin loaded ODEL1 and ODLE2 (two optimized products) is published in our previous report except mechanistic understanding of permeation behavior (Altamimi et al., 2021a).

HSPiP-based predictive Hansen solubility parameters (HSP) such as dispersive energy (δ_d), polarity energy (δ_p), and hydrogen bonding (δ_h), are well explored to understand interaction between solute and solvent. Moreover, the theoretical prediction was also established to identify possible interactions between topical formulations (cream, gel, and lotion) and human skin (Altamimi et al., 2021a; Cormier et al., 2004; Hussain et al., 2016). Abbott, 2012 was the first to report the values of δ_d, δ_p, and δ_H values as 17, 8, and 8, respectively, for human SC. These are important parameters to understand the mechanistic events of permeation by interactions between the skin cells and vesicles (Abbott, 2012; Altamimi et al., 2022; Ezati et al., 2020). Literature revealed intriguing results about the interaction of hydrophilic and lipophilic drugs with nail plate and the hoof membrane in terms of HSP values (Hussain et al., 2020; Hossin et al., 2016). Generally, HSP values of skin change depending on the physiological and pathological conditions (diseased, normal, and traumatic) (Hossin et al., 2016).

SEM (scanning electron microscopy) and fluorescence microscopy visualize and track microscopic changes after topically applied products, respectively. Moreover, the understanding of molecular changes after treatment, can be studied using FTIR spectroscopy (Fourier Transform Infra-Red spectroscopy) and DSC (Differential Scanning Calorimeter) techniques for comparative assessment (control versus treated skin). FTIR can be used to investigate molecular variation of the treated skin tissue by measuring spectral changes of rodent dermal skin after irradiation and comparing it with the control group. A normal skin elicits a typical absorption FTIR spectrum (carbohydrates, lipids, and proteins) and a characteristic endothermic peak after treatment with liposomal formulation (Alkilani et al., 2015; Hosseini et al., 2021). Fluorescence microscopy provides visual inspection (visible under the dye probed spectroscopy) of the extent of penetration into the skin. Thus, we reported mechanistic understanding of ODEL1 mediated reversible changes, interaction with skin, and penetration across SC of rat skin as comparative assessment. The work is the state-of-the-art mechanistic assessment using Hansen parameters and instrumental techniques not reported so far. A detailed insight into permeation of DA loaded elastic liposomes was explored and explained as well in rat skin model. The objective was complete understanding of permeation mechanisms and interaction of vesicles with the skin after application. The study was extended part of our previous report (Altamimi et al., 2021a). Thus, optimization and subsequent mechanistic understanding of permeation of DA loaded vesicles would be informative to reader engaged in sustained delivery of DA to control the aforementioned diseases.

2. Materials and methods

2.1. Materials

Desmopressin acetate (DA, > 99.8 %) was purchased from Jinlan Pharm Drugs Technology Co., Limited (China). For aqueous solvent, milli-Q water was employed. HSPiP (version 5.0.2) software was procured from Dr. techn. Charles M. Hansen Jens Bornøsvej 162,970 Hørsholm Denmark (online model of purchase). Tissue fixative poly-L-lysin, tween 80, and rhodamine 123 were purchased Sigma (USA). DSC pan was procured for thermal analysis of skin samples from Perkin Elmer (DSC-4000 Perkins Elmer (Waltham, MA, USA). Phospholipid (phospholipon 90H) and sodium cholate were procured from Lipoid, GMBH, Frigenstrasse 4, D-67065, Ludwigshafen, Germany and CDH Fine Chemical, Mumbai, India, respectively. Ethanol served as plasticizer and it was purchased from Sigma Aldrich, Mumbai. Span 80 and tween 80 were obtained from Loba Chemie Pvt. Ltd. 107, Wodel House Road, Mumbai, 400,005, India. Formulations ODEL1, ODEL2, and the drug solution (DS) were in house products.

3. Methods

3.1. Composition and characteristics of optimized elastic liposome (ODEL1-R123 and ODEL2-R123)

Two optimized products, ODEL1-R123 and ODEL2-R123, were obtained from in-house laboratory (Altamimi et al., 2021a). In brief, ODEL1 is comprised of 285 mg of phosphatidylcholine (PC) and 115 mg of sodium cholate (SOC), which serves as an edge activator. The colloidal milky suspension of elastic liposomes was obtained by hydration in phosphate buffer solution (PBS, pH 7.4) containing 2 mg of DA and 7 % of ethanol (plasticizer). Similarly, ODEL 2 contained 272 mg of PC, 100 mg of SC, 2 mg of DA, and 7 % ethanol in PBS (1 mL). These were reformulated following the same procedure as reported before with rhodamine 123 (0.05 %) dye as a fluorescence probe to track the extent of penetration across SC (Altamimi et al., 2021a). The probe solution (0.05 %) was freshly prepared in distilled water as a control. The suspension (DS) was prepared in distilled water containing 0.1 % carboxymethyl cellulose sodium (Na-CMC) as a suspending agent. The reformulated ODEL1 and ODEL2 were designated as ODEL1-R123 and ODEL2-R123, respectively.

ODEL-R123 and ODEL2-R123 were formulated following the method reported before (Altamimi et al., 2021a). Lipid, surfactant (span 80), and rhodamine 123 were dissolved in chloroform whereas aqueous phase (phosphate buffer solution as hydrating medium) contained desmopressin acetate and hydrophilic surfactant (if present). Initially, round bottom flask (completely dried) was used to make a thin film of the organic phase over rotary evaporator. The developed film was confirmed visually. The film was hydrated using PBS solution containing DA and water soluble components such as ethanol (7–10 %) and tween 80 (if required). Hydration step resulted in the formation of colloidal milky suspension of ODEL1-R123 and ODEL2-R123. The prepared formulations were stored in freeze to activate vesicles.

For gel formulations, carbopol 934 (1 g) was completely dispersed into cold water (100 mL). The dispersion was vigorously stirred to dissolve the polymer. Basic triethanolamine (0.3 mL) was added to initial gelling process. Final pH was measured using a digital pH meter. Consistency was manually tested. ODEL1-R123 and ODEL2-R123 (1 g) were individually dispersed into the freshly prepared gel (1 g) to get homogeneous gel formulation. These formulations were labeled as ODEL1-gel and ODEL2-gel accordingly.

3.2. Estimation of HSP values using HSPiP

HSPiP is a software based on theoretical understanding of innate total cohesive energies present in a material. These cohesive energies are

material specific and are expressed as a set of three partitioned cohesive energies: dispersion energy (δ_d), polarity energy (δ_p), and hydrogen bonding energy (δ_h). Notably, polar energy, hydrophobic hydrocarbon-based London dispersive energy, and H-bonding are effective molecular interacting forces to deal with polar materials (Daisuke et al., 2017). HSP values were estimated for each component of ODEL1, ODEL2, and the formulations (ODEL1 and ODEL2) using SMILE file as shown in Table 1. Similarly, the reported values of HSP of human skin cadaver from various literature database have been included in the same table as a reference. In general, a solute interacts with a solvent with collective interactive forces, including dielectric constant, H-bonding ability, van der Wall force of attraction, London forces, and cohesive-adhesive force. Based on the composition of ODEL1 and ODEL2, HSP values were estimated. The hydrating media (PBS) was considered as water for HSP estimation (δ_d, δ_p, δ_h, δ_t, and mVol) in HSPiP program. HSP values of human skin were used as a target to achieve which is discussed in the experimental and discussion section. R_o and R_a represent 3-dimensional sphere diameter and space parameter for the studied compound in HSPiP, respectively. RED (relative energy difference) is used to flag a solvent as good or bad depending on its value from unity (R_o to R_a). RED is used to differentiate a good solvent from a bad solvent using the pooled database. RED <1 is considered as a good solvent and vice versa. Moreover, a solute interacts effectively if the difference of any HSP value is close to zero or minimum. Similarly, if a compound, solvent or formulation possesses HSP values close to the HSP values of skin (obtained from HSPiP manual), it can be considered efficiently interactive for permeation across skin (δ_d of skin – δ_d of components/ODEL = close to zero, δ_p of skin – δ_p of components/ODEL = close to zero, and δ_H of skin – δ_H of components/ODEL = close to zero) (Ezati et al., 2020; Khan et al., 2024).

3.3. Preparation of rat skin for morphological changes

An attempt has been made to investigate the impact of ODEL1-R123 and the drug solution containing rhodamine 123 (DSR123) on the treated skin of rats. Wistar rats of both sexes were used in the study. Moreover, these animals were 5–6 months old weighing approximately 300 g. Therefore, animals were received from the Department of Pharmaceutics, College of Pharmacy, King Saud University after obtaining the required ethical approval (KSU-SE-20-64). Animals were in-housed under air-conditioned room with free access to food and water. The experimental procedure and protocol were designed as the ARRIVE guidelines (guideline for animal care, NC3Rs). Rats were grouped as A, B, C, and D. The group A was untreated and served as the control. The group B, C, and D received ODEL1-R123, ODEL2-R123, and DSR123, respectively. We avoided to use chemical cream or gel to remove hairs. Therefore, we used razor to remove these hairs. In this step, we cared to avoid any razor based cut or surgical lesion. To observe micro changes, we observed under magnifying glass.

Table 1
A summary report of HSP of desmopressin, excipients, the optimized formulation, and SC of humans.

Name	HSP values estimated in HSPiP ($MPa^{1/2}$)				
	δ_d	δ_p	δ_H	δ_{total}	HLB
DES	20.6	31.9	18.2	42.2	–
#PC	16.1	6.4	9.1	19.57	–
**Skin	17.5	12.6	11.1	24.24	
Ethanol	15.59	9.05	18.3	25.89	–
Span-80	16.69	6.09	12.37	–	4.3
SC	17.6	5.9	9.8	21.0	16.8
Tween-80	16.7	6.5	9.4	20.0	15.0
Water	15.48	16.1	42.0	48.0	–
ODEL1	15.6	14.97	2.4		
		SMILE input parameter			mVol
DA	c1ccc(cc1)C[C@H]2C(=O)N[C@H](C(=O)N[C@H](C(=O)N[C@@H](CSSCCC(=O)N[C@H](C(=O)N2)Cc3ccc(cc3)O)C(=O)N4CCC[C@H]4C(=O)N[C@H](CCCNC(=N)N)C(=O)NCC(=O)N)CC(=O)N)CCC(=O)N				778.9
#PC	CCCCCCCCCCCCCCCCC(=O)OC[C@H](COP(=O)([O-])OCC[N+](C)(C)C)OC(=O)CCCCCCC/C=C\CCCCCCCC				–
Skin-SC	Not available				–
Ethanol	CCO				58.2
Span-80	CCCCCCCCC=CCCCCCCCC(=O)OCC(C1C(C(CO1)O)O)O				428.0
SC	C[C@H](CCC(=O)[O-])[C@H]1CC[C@@H]2[C@@]1([C@H](C[C@H]3[C@H]2[C@@H](C[C@H]4[C@@]3(CC[C@H](C4)O)C)O)O)C. [Na]				389.0
Tween-80	CCCCCCCCC=CCCCCCCCC(=O)OCCOCC(OCCO)C1OCC(OCCO)C1OCCO				1313.9
Water	OH				18.0

Note: DA = desmopressin acetate, HLB = Hydrophilic lipophilic balance, #PC = Phosphatidylcholine (Hansen, 2007)**. *Reference. **Hansen solubility HSPiP software manual. mVol = Molecular volume, SC = Sodium cholate.

3.4. Assessment of molecular stretching using ATR-FTIR

Rats were treated according to the protocol with the exception of the control group (Godin and Touitou, 2007). The test sample (100 mg) was applied on a thin film to the marked area (1.0 cm^2) using a spatula. The epidermal side of the skin surface was used to load the sample. The applied area was protected from washing or animal licking for 12 h using a plastic mesh. After 12 h, the treated skin (an area of 1.0 cm^2) was excised after ethical sacrifice (cervical dislocation) of the respective groups. The excised rat skin was cleaned and made free of hairs. The tissue sample was then placed on a glass slide. The adhered sample was removed before observing the changes under microscopy and ATR-FTIR. The skin samples were cut into a disc shaped circular shape to put as such in the ATR-FTIR (Model Bruker Alpha II, Bruker Alpha, Germany) sample holder coupled with an internal reflection element of Platinum Diamond (Platinum Diamond Ref#1 24c78F972D). The tissue samples were analyzed and compared against the control (untreated) in terms of IR spectral assessment. This assessment involved scanning (scan numbers of 16) between 4000 and 400 cm^{-1} to examine bond vibration and stretching associated with skin composition (functional groups of skin protein, carbohydrates, and lipids) with resolution of 4.0 and the entrance/exit faces angle of 45°.

3.5. Assessment of thermal behavior

DSC was utilized to observe the thermal changes that occurred in previously treated and untreated control samples. The excised rat skin (stratum corneum of abdominal rat skin) was cleaned and made free of hairs. The stratum corneum was removed using the most robust and common tape stripping method (Alkilani et al., 2015). This was carried out to compare the effects of the treatment with the control group. A precise amount of the tissue sample (2–3 mg) was extracted from the treated area, following a reported method by our research group (Altamimi et al., 2021a). The sample was air-dried overnight without any heat treatment. Each sample was then separately assessed using a DSC-4000 (DSC-4000, Perkin Elmer, USA) (Hussain et al., 2017). The dried skin sample was fully crimped inside an aluminum pan and placed inside the furnace chamber. The sample was heated at the rate of 10 °C/min up to 250 °C.

3.6. Fluorescence microscopy

Each treated sample contained rhodamine 123 as a probe to monitor the extent of permeation across SC layer. The samples ODEL1-R123, ODEL2-R123, and DSR123 contained equivalent amount of the drug. DSR123 was used for comparative assessment. The study was conducted following the method reported by Jian, where an ethosomal product was used to treat rat skin using rhodamine123 as a probe (Jain et al., 2007). Skin samples (free from hairs) were collected after 12 h post-treatment. The collected tissues were immediately sliced into fine pieces using a

microtome (Leica CM3050 S cryostat, Leica Microsystems) and a fixative (Tissue-Tek O.C.T. compound, Torrance, USA). The tissue samples were properly sliced as per the reported method (Alshammari et al., 2019). The sliced tissue was fixed over a glass slide (Fisher scientific) and then dried overnight. Finally, the sample specimen was visualized (excitation and emission wavelengths of 488 nm and 560 nm, respectively) under a Zeiss LSM-780 fluorescence microscope (equipped with 100 W Mercury Lamp) to observe the extent of penetration across skin epidermis (Mirgorodskaya et al., 2017; Lei et al., 2022).

3.6.1. Assessment of microscopic structural changes

The same sample used in the fluorescence study was used for SEM. However, the tissue specimen was coated with a gold coating agent (at 20 mA for 60 s) using a fine coat ion sputter coater. The sample was made enough conductive so that it can be easily visualized (Zeiss EVO LS10; Cambridge, United Kingdom). The sample was scanned under high magnification to record desired micrographs during surface morphological examination (Hussain et al., 2016). The study provides insights into the effect of the formulation on the histology of skin after treatment and the vesicle-skin interaction.

4. Result and discussion

4.1. Excipients and HSP based predictive explanation for interaction

Notably, the effectiveness of the drug entrapment, vesicle-skin interaction, and relative formation of micelle depends upon various factors such as the drug properties, molecular structure of surfactant/lipid, formed vesicles shape, the presence of auxiliary components (ethanol) in the formulation, and solution conditions (pH, ionic strength, and aqueous volume) (Mirgorodskaya et al., 2017). ODEL1 and ODEL2 were associated with the vesicle size values as 121.6 nm and 138.2 nm, respectively whereas these have zeta potential values of – 27.9 and – 33.7 mV, respectively. Notably, particle size distribution pattern values were approximately similar (PDI of ODEL1 as 0.15 and 0.18 for ODEL2) as before (Altamimi et al., 2021a). % EE values for ODEL1 and ODEL2 were 81.4 % and 73.9 %, respectively with insignificant difference from the reported values (Altamimi et al., 2021a). Both products (ODEL1 and ODEL2) were optimized based on high desirability parameters (D_i = 0.924 for ODEL1 and 0.913 for ODEL2). ODEL1 was associated with extended %DR (75 %) for a period of 12 h and high permeation flux (J_{ss}) (0.53 μg/cm^{2}h) whereas ODEL2 exhibited %DR of 69 % and J_{ss} of 0.31 μg/cm^{2}h which may be attributed varied composition and formulation characteristics (Altamimi et al., 2021a). Notably, ethanol content was constant at 7 % to avoid micellar formation during the hydration step (Pal et al., 2019). The hypothesis was that lipid-based vesicle can interact with the cellular surface in various ways to enhance permeation. This includes follicular transport, lipid-lipid fusion, passive and active transport, and a concentration gradient established by trans epidermal water loss (TEWL). Elastic liposomes containing ethanol may cause reversible changes in the skin, deformability in vesicles, and vesicle size reduction (Pal et al., 2019). To validate the hypothesis, FTIR, DSC, fluorescence microscopy, and SEM techniques provided substantial evidences to justify the proof of concept. The results were correlated to the predicted HSP values as supportive finding to understand mechanistic aspect of the interaction (cohesive energies) of ODEL1-R123, ODEL-R123, and DSR123 with rat skin for optimal permeation parameters as explained in subsequent paragraph (Altamimi et al., 2021a).

From Table 1, it is evident that DA is a highly polar (δ_p = 31.9 MPa$^{1/2}$), dispersive (δ_d = 20.6 MPa$^{1/2}$), and capable to form hydrogen bonds (δ_h = 18.2 MPa$^{1/2}$). Therefore, the drug expected to be preferably entrapped into the inner aqueous compartment (δ_p = 16.1 MPa$^{1/2}$) of vesicle rather than the lipid bilayer. Considering the HSP values of PC, the lipid bilayer is least suitable for DA interaction for its loading into it. The overall calculated HSP values of ODEL1 were found to be 15.7 MPa$^{1/2}$ (δ_d), 12.7 MPa$^{1/2}$ (δ_p), and 28.6 MPa$^{1/2}$ (δ_h). Thus, the ODEL1 vesicle interacts primarily through polar energy (polarity interaction) and dispersion power as evidenced by the close HSP values of the skin δ_p (12.6 MPa$^{1/2}$) and δ_d (17.5 MPa$^{1/2}$). These theoretical interactive forces and other mechanistic factors for improved permeation can be collectively considered as combined efforts working tandem. The formulation composition (ethanol and surfactant) and gel based hydration energy are additive forces for improved permeation of the loaded drug across SC. Ethanol served as a plasticizer in the vesicle, enabling the ultra-deformed vesicle to be squeezed into the skin through tiny and tortuous pathways of corneocytes (Pilch and Musiał, 2018). The surfactant extracts surface lipid to cause reversible temporary perturbation. These surfactant monomers can interact with the inner protein-rich areas within the normal SC to get diffused via the lipid portion and subsequent binding to the proteins (δ_p-δ_p, δ_d-δ_d, and δ_h-δ_H interactions between the surfactant and skin). The bound surfactant monomers cause protein denaturation and subsequently swelling of SC for enhanced drug permeation (Ananthapadmanabhan et al., 1996; Barel et al., 2009).

Elastic liposomes, free from cholesterol, exhibit maximum flexibility, deformability, and fluidity. These unique features enhance permeation compared to conventional liposomes. These vesicles are designed to be squeezed through tortuous microscopic pathways (microlamellar spaces) or pores (size 1/10th of vesicle size) to deliver the drug to the dermal region for systemic availability (Benson, 2006). The large inner chamber (aqueous) has dual functions: (a) loading the hydrophilic drug and (b) compensating for transepidermal water loss (TEWL) to maximize drug permeation and skin protection (Benson, 2006). The SC, which is the densest and most compact layer (15–20 layers of 10–15 μm thickness), serves as a physiological first-line barrier and rate-limiting barrier for transdermal delivery. Hydration-mediated swelling increases SC thickness up to 40 μm, subsequently widening the intracellular tortuous spaces available for vesicle (squeezed under hydration), and differential driving forces operating in tandem (Christophers and Kligman, 1964; Scheuplein, 1967).

Considering the HSP values (δ_d, δ_p, δ_h, δ_t) of the explored excipients, the drug, and skin, the optimized formulation was expected to interact maximally if the HSP values achieved are close to the skin (δ_d of skin ~ δ_d of the vesicles; δ_p of skin ~ δ_p of the drug; δ_H of skin ~ δ_H of the drug). These forces (London force, dispersion power, and hydrogen bonding capability) act collectively after transdermal application.

These predicted values support the possible interactions between the vesicle and skin components. Ezati et al. reported "R_{skin}" in the range of 4.0–6.6 (obtained from Hansen manual) (Ezati et al., 2020). In contrast, the calculated $R_{odel\text{-}1}$ value for ODEL1 (considering whole suspension/mL) is approximately 17 which is quite high from real skin "R" value. The interacting vesicles at the skin surface contain about 3–4 % water (as inner vesicle volume), 7 % ethanol as a plasticizer, and PC as a lipid for lipid-lipid interaction. These collectively function as a driving factor for permeation towards the inner region across SC layer (Perkins et al., 1993). Notably, ethanol and surfactants are good permeation enhancers due to extracting ability of skin lipid and perturbation. These changes may be attributed as temporary and reversible. Liposomes contains higher content of cholesterol (25–30 %) in the lipid bilayer making it in ethanol or hexane. However, mixture of ethanol and hexane (50:50) worked as suitable solvent for solubilizing cholesterol in the lipid matrix (Hansen and Andersen, 1998). Thus, a slight rigid nature of liposomes bilayer may be attributed to insoluble nature of cholesterol in the lipid matrix of liposomes making it different from elastic liposomes (free from cholesterol and highly deformable vesicle). It is noticeable that the permeation across skin takes place mainly through intra-and intercellular routes. These vesicular systems penetrate the skin effectively via the intercellular pathways since the lipid bilayer is highly flexible for its deformability. The deformed vesicles easily cross the intercellular spaces (Souto et al., 2021).

4.2. Stretching and bond vibration using ATR-FTIR

Fig. 1 portrayed characteristics peaks for the control and treated rat skin and the results were compared qualitative and quantitative. Functional groups of basic components of skin are sensitive to IR irradiation in terms of bond vibration and stretching. A normal skin elicits a typical absorption spectrum (carbohydrates, lipids, and proteins) with characteristic absorption peaks of 2854–2952 cm^{-1}, and 1400–1450 cm^{-1} (C—H stretching), for lipids and carbohydrates (C—H bending), respectively. Moreover, skin proteins are related with CN (1550 cm^{-1}), C═O (1650 cm^{-1}), and C═OOR (1750 cm^{-1}) stretching (Hosseini et al., 2021). These unique peaks are the finger print of the basic components of skin. By inspecting peaks at 2922.0 and 2852.11 cm^{-1}, it can be related to C—H stretching of the lipid component of rat skin whereas the prominent peaks at 1451.21 and 1404.0 cm^{-1} confirms C—H bending vibration of saturated proteins. Detail insights of the ester bonds present in phospholipids and amide-I of biological membrane are associated with three consecutive peaks at 1542.76, 1629.72 (amide-I peak), and 1742.75 cm^{-1} (amide-I peak). The functional groups involved are – CN, C═O (amide-I peak), and C═OOR (stretching vibration) (Fig. 1A). These characteristics obtained from control were used to compare against the treated skin. These peaks (stretching and bending) are in good agreement with the findings reported before for the surface lipids and proteins of rat skin (Alkilani et al., 2015). The DS treated skin exhibited no significant changes in the characteristic peaks associated with the surface proteins and lipids, as these were comparable as the peak patterns of the control. This confirmed no remarkable interaction with the surface of rat skin (Fig. 1B). Observing the characteristics peaks of blank ODEL1 (Fig. 1B) and the optimized ODEL1 (Fig. 1C), it is apparent that there were significant variations in stretching and vibrations as compared to the untreated skin sample (Fig. 1A). Notably, the gel formulation elicited an intense peak pattern compared to the untreated skin sample. This is attributed to gel-mediated hydration, swelling, and H-bonding with the polar functional groups of the surface proteins, resulting in reasonable interactions to cause reversible changes (Fig. 1D) in skin protein (peaks at 3288.07 cm^{-1} and 2858.29 cm^{-1}). The observed low-frequency peaks at 1089.24 cm^{-1} (untreated skin), 1074.44 cm^{-1} (ODEL1-Gel), 1074.33 cm^{-1} (ODEL1), and 1038 cm^{-1} (drug solution) are associated with the vibrational modes of CH_2OH functional groups due to C—O stretching and C—O bending of skin carbohydrate and symmetrical stretching of ionized PO^{2-} group. These slight variations from the untreated group indicted reversible and interaction after topical application (Parker, 1993). Moreover, the prominent peaks observed around 1240 cm^{-1} (1237.58, 1241.12, 1238.58 cm^{-1}) are related to asymmetrical stretching PO^{2-} group compared to untreated group (1236.66 cm^{-1}). ODEL1-Gel exhibited lower frequencies (< 1000 cm^{-1}) completely different from the untreated group, indicating significant interaction with protein and carbohydrates of skin matrix (SC layer) as shown in (Fig. 1D). Thus, various modes of interactions (cohesive energies, electrostatic energy, dispersion energy, Van der Waals interaction, polar due to PO^{2-} group, and H-bonding) exist between the components of the formulation and skin composition. There is combined impact of these interactions on permeation properties for vesicles working in tandem. These stretching and vibrational modes were attributed to reversible perturbation occurring due to London forces, hydrogen bonding, reversible bond breaking, hydration for swelling, and lipid-lipid dissolution working in tandem (Hansen and Andersen, 1998).

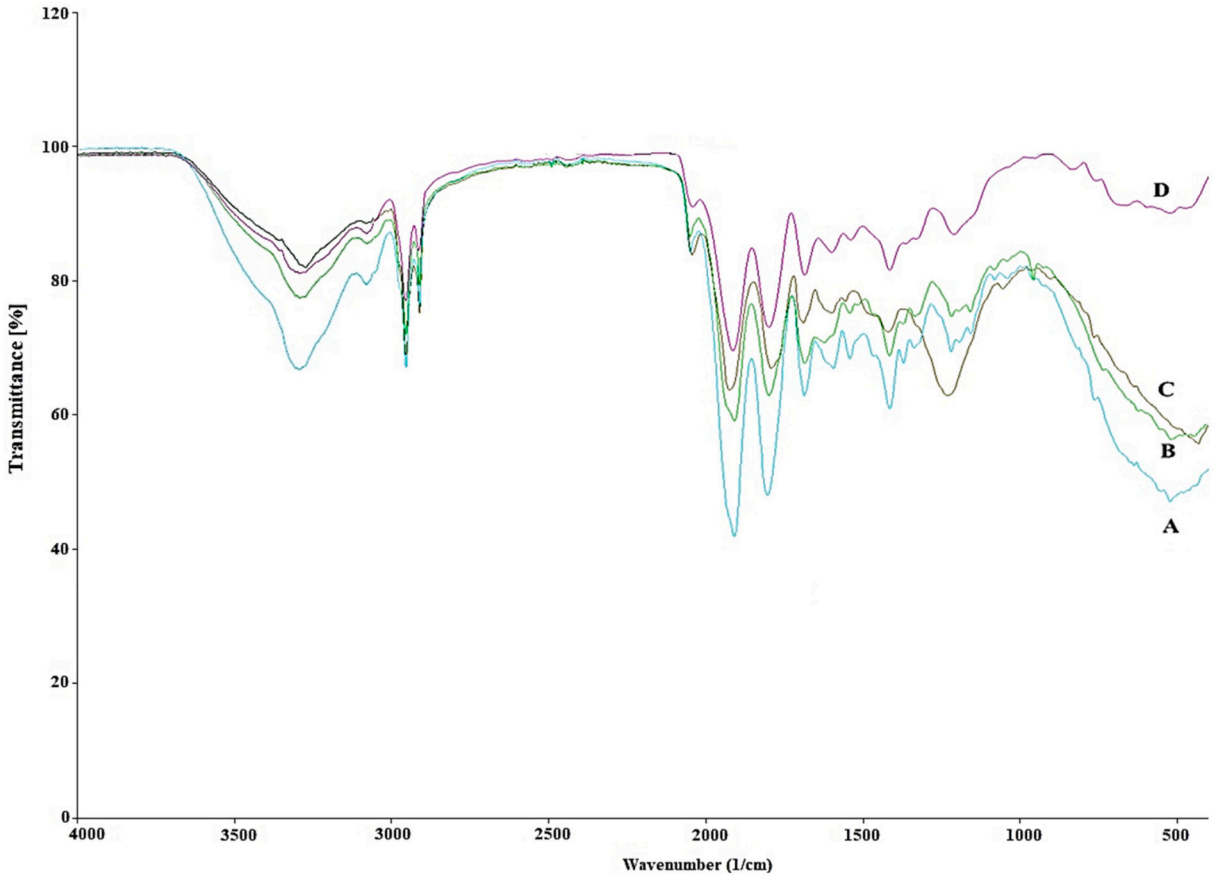

Fig. 1. Fourier Transform Infrared (FTIR) study for the treated and untreated rat skin samples: (A) the control untreated rat skin, (B) blank ODEL1 treated skin, (C) the optimized ODEL1 treated rat skin, and (D) ODEL1-Gel treated rat skin.

4.3. Assessment of thermotropic behavior of the treated and control skin

To investigate the impact of ODEL1 on permeation behavior across SC layer, it was required to study thermotropic nature of the treated and the control (untreated) skin using DSC tool. Human skin cadaver DSC exhibits a remarkable endothermic peak at 84 °C (fusion point), which may shift to higher values (shifted to ~130 °C and 171 °C) after treatment with liposomal formulation (Alkilani et al., 2015). Goh et al. reviewed several interesting findings about the thermal induced endothermic peak in human stratum corneum and porcine skin. The authors highlighted four prime peaks (T_1, T_2, T_3, and T_4). Among these T_1 (40 °C) and T_2 (70 °C) correspond to lipid related reversible changes after surfactant application whereas T_3 (80 °C) and T_4 (100 °C) are related to irreversible protein denaturation (Kirjavainen et al., 1996; Goh et al., 2022).

The results of DSC are presented in Fig. 2A-D. Fig. 2A and B indicate the untreated control and DS treated rat skin, respectively. Similarly, Fig. 2C and D indicated blank and ODEL1 treated rat skin, respectively. Observing these images, the treated skin exhibited significant structural changes (reversible) due to carrier mediated interaction with the skin composition and aqueous attributed hydration. In this study, the disappeared or shifted characteristics peaks at 67 and 79 °C peaks indicate SC lipid amalgamation (polar head disruption) related to keratin of the skin (Kirjavainen et al., 1996; Goh et al., 2022). Thus, ODEL1 profoundly interacted with the skin surface to deliver hydrophilic DA across SC layer through lipid-lipid interaction (reversible) and irreversible denaturation of keratin protein (Kirjavainen et al., 1996; Goh et al., 2022). It was quite critical to confirm the surfactant mediated phase change between hexagonal and orthorhombic crystals of intercellular lipids. However, the obtained characteristics peaks at 67 and 79 °C peaks are closely related to 80 °C of protein and lipid phase changes due to the combined impact of ethanol, lipid-lipid amalgamation, and surfactant present in the formulation (Fig. 2A and B within rectangle) (Goh et al., 2022). Fig. 2C is ODEL1 (blank formulation) treated thermogram wherein a slight change in characteristic peak at 80 °C was shifted to 84 °C (as shown in rectangle) which may be attributed to the composition mediated transition. Interestingly, ODEL1 treated skin elicited the loss of this characteristic peak (the absence of 80 °C) due to significant interaction with the skin components (Fig. 2D within rectangle). All DSC thermograms revealed a prominent endothermic peak in the range of

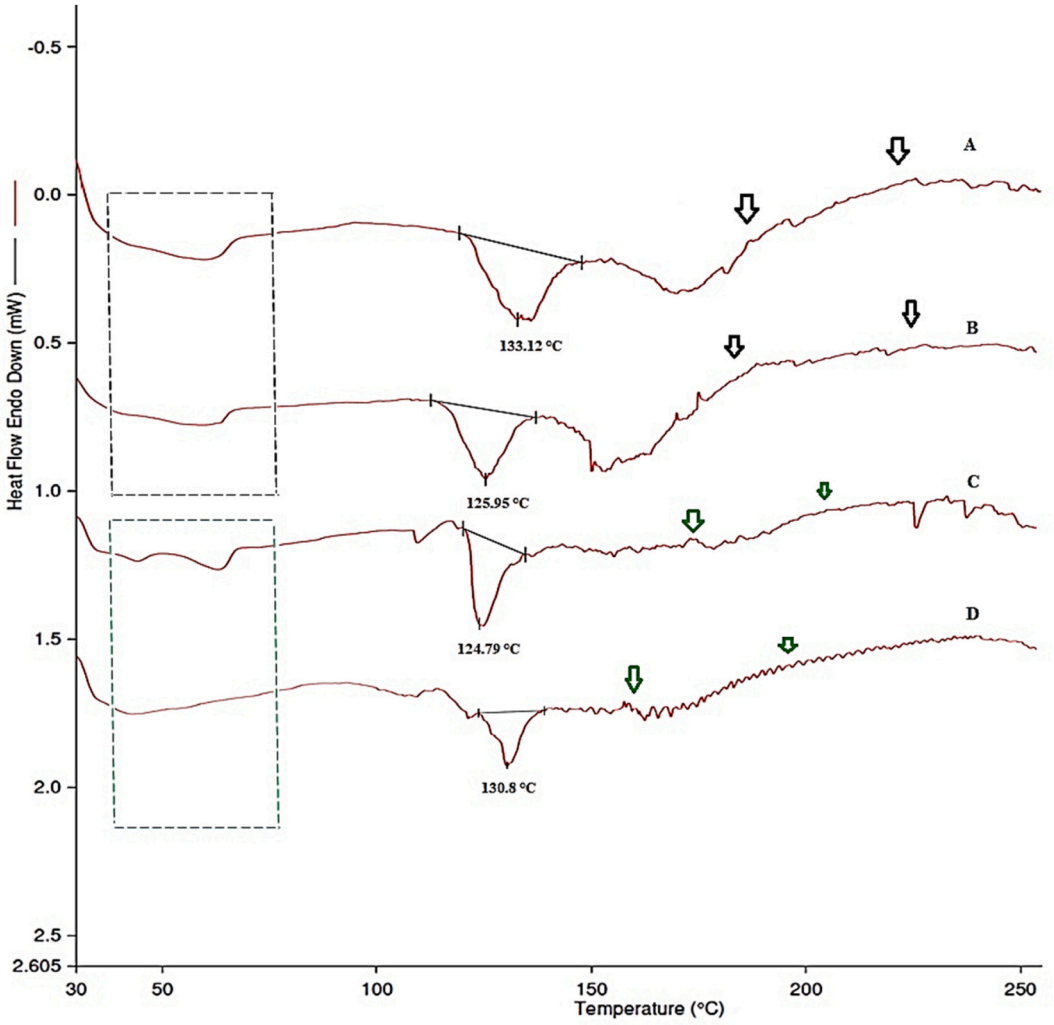

Fig. 2. Differential scanning calorimeter (DSC) of the control (untreated) and treated rat skin.(A) the control rat skin with characteristic peaks at 133.12 °C, 82.5 °C, and 65 °C, (B) DS treated rat skin with characteristic endothermic peaks (slight variation) similar to the control, (C) blank ODEL1 treated rat skin with a slight variation in thermal endothermic characteristic peaks (a shift from 80 °C to 84 °C) as compared to the control (green rectangle with broken lines), and (D) ODEL1 exhibited substantial changes in thermal behavior as evidence with the changed endothermic thermal peaks (absence of peaks at 65 °C and 84 °C) and heavily noised curve beyond 150 °C (green arrow indicated noise due to high perturbation). Encircled area indicated thermal transitions of SC-lipids, lipoprotein of SC, and denatured SC protein attributed to ODEL1. The pattern exhibited by black arrows suggests intact skin surface (stratum corneum) due to the lack of any changes. (For interpretation of the references to colour in this figure legend, the reader is referred to the web version of this article.)

124–134 °C, which is related to the highly crystalline SC (flat keratinized corneocytes embedded in intercellular lipid matrix) of the skin (Alam et al., 2016). In human cadaver skin, it appears nearly at 130 °C (Kalita and Das, 2018). In this study, these values were found to be as 133.12 °C, 125.95 °C, 124.79 °C, and 130.8 °C, for untreated control skin, DS treated skin, blank treated skin, and ODEL1 treated rat skin, respectively. The treated rat skin executed relatively lower than the untreated skin، suggesting that SC layer is reversibly perturbed by the applied formulations. Notably, the skin is generally composed of intercellular skin lipid, proteins associated with lipids (lipoproteins), and highly crystalline denatured SC protein. The characteristic endothermic transitions of untreated abdominal rat skin in DSC thermogram are observed at 65 °C (transformation of lipid from lamellar state to disordered state), 82.5 °C (protein lipid complex melting), and 115–130 °C (protein irreversible denaturation) due to the melting of the intercellular lipids, lipoproteins, and the denatured SC protein, respectively (Salimi et al., 2016). Formulation attributed any reversible or irreversible structural changes (disruption, perturbation, and lipid extraction) result in significantly diminished lipid or protein transitions (Dreher et al., 1997; Ahmed and Rizq, 2018). Fig. 2A and B (suspension) elicited prominent endothermic transition peaks at 66.9 °C (enclosed within black broken square line) due to the intercellular lipid bilayer of SC. DS (suspension) could not attributed substantial changes in the lipid bilayer of SC as observed in the result and it is similar to the untreated control (Fig. 2A). However, blank ODEL1 attributed substantial changes in the intercellular lipid bilayer of SC as evidenced with two transitions observed (Fig. 2C, enclosed within green broken line square). This suggested ODEL1 mediated marked changes in lipid organization of SC layer for enhanced permeation of elastic liposomes. Interestingly, (Fig. 2D) showed the merged and broad characteristic endothermic peak at 65 °C indicating complete internalization and fusion of the lipid bilayer of the intercellular lipids. Moreover, the remarkable transition peaks observed at 115 °C in (Fig. 2C and D) are related to disruption of protein-associated lipids of SC layer caused by the elastic vesicles of ODEL1. These enforced changes can be correlated to the components of ODEL1 such as ethanol (as plasticizer), PC (lipid-lipid amalgamation), and surfactant/co-surfactant (perturbation and structural changes).

4.4. Fluorescence microscopy of treated skin

Vesicular systems are lipid bilayer systems that can interact with the biological surfaces after transdermal application. These are widely used for safety, sustained drug release property, and improved clinical efficacy for various drugs. Elastic liposomes are considered as superior to conventional liposomes due to deeper penetration, high deformability, and systemic drug access after transdermal application (Ahmed and Rizq, 2018). The penetration of rhodamine 123 probed ODEL1-R123, OLEL2-R123, and DSR123 are exhibited in Fig. 3A-C. Fig. 3A shows the DSR123 treated rat skin, where the upper section (SC and epidermis) of rat skin revealed intensified region due to localized penetration of the dye only (aqueous nature of the dye solution). The deeper region of the dermal area is free of intensity and the absence of the dye due to the lack of any penetration enhancer or nanocarrier. Fig. 3B and C indicate ODEL1-R123 and ODEL2-R123 treated rat skin, respectively, where the degree of penetration was substantially high (intense fluorescence intensity in the dermal region) as compared to the control (Fig. 3A). This was correlated to the composition (ethanol content, lipid, and surfactant) of elastic liposomes and formulation characteristics (small size vesicles and ultra-deformability and flexibility). The highly intense fluorescence is attributed to ethanol-mediated surface perturbation and deformed vesicle capable to be squeezed (ethanol triggered increased flexibility in lipid bilayer of vesicles) across SC layer following tortuous pathway of corneocytes and basal layer (Ramzan et al., 2024). These topological changes are temporary to make its pathways (intracellular and intercellular pathways) for vesicles permeation after application. The changes that occur allow the drug-loaded vesicles to permeate across SC layer for enhanced drug permeation flux and the drug deposition. Moreover, follicular route of permeation also plays an alternative pathway for improved drug permeation. However, this route is insignificant due to limited surface area (0.1 %) compared to others. Thus, the combined effects of surfactant, ethanol, and vesicle working in tandem have facilitated the permeation of DA after transdermal application to execute therapeutic benefit.

4.5. Microscopic visualization of vesicles-skin interaction: SEM technique

The study supported the findings of the FTIR, DSC, and fluorescence results. The observed changes were compared against the untreated

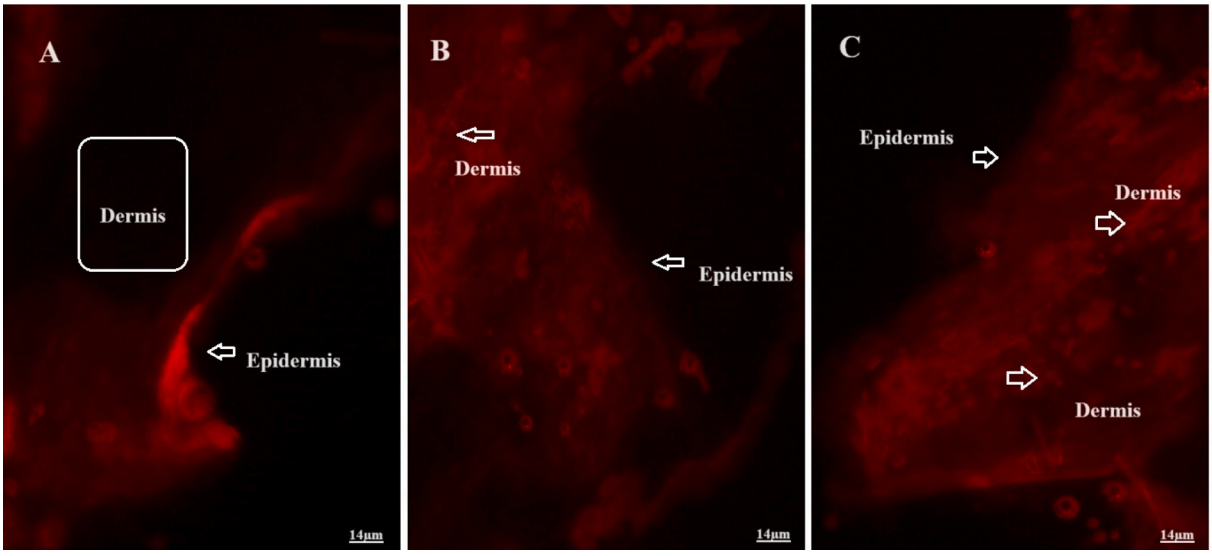

Fig. 3. Representative images of rat skin visualized under fluorescence microscopy: (A) Rat skin treated with DSR123 for 4 h elicited confined content of dye to the epidermis surface only and dermis did not show any fluorescence (marked rectangular area), (B) ODEL1-R123 treated skin revealed permeated amount of the drug loaded formulation towards dermis, and (C) ODEL2-R123 treated rat skin exhibited relatively high permeation of the applied formulation after transdermal application as evidenced with high degree of fluorescence intensity in dermal area.

control group as illustrated in Figs. 4A-D. The microscopic photographs revealed structural changes post-treatment, which could be attributed to the lipid and surfactant mediated perturbations. The presence of ethanol (7 % *v*/v) induced the reversible changes in the anatomical architecture of skin surface such as protein and lipid of SC layer. Considering safety concern (maximum daily exposure), it was optimized and recommended to 7 % in each formulation (Utreja et al., 2011). Currently, EU directive discussed the risk management (EU cosmetics directive 76/768/EEC) for maximum recommended concentration of ethanol (20 mg/kg) in the finished cosmeceuticals (Lachenmeier, 2008). Moreover, higher content of ethanol disrupted the vesicles and the lipid bilayer as explored in the lab. Therefore, we finally fixed at 7 %. In a literature, ethanol content was explored in the elastic liposomes for the topical delivery of paclitaxel (Utreja et al., 2011; Altamimi et al., 2021b; Barry, 1987). It mainly served as vesicle plasticizer whereas the surfactant primarily worked as skin lipid extraction.

Inset of Fig. 4A exhibited normal anatomical SC layer and surface morphology (smooth and surface margin) of rat skin scanned at varied magnification. Anatomically, SC (compact corneocytes cells) is a highly compact first-line physiological barrier of the epidermal surface, as observed in Fig. 4A. Fig. 4B represents DS treated sample with no substantial changes in surface morphology as compared to the control. This was expected due to the absence of any permeation enhancer or surfactant. On the other hand, ODEL1-R123 and ODEL2-R123 revealed significant variations in surface morphology as compared to the control, which may be attributed to vesicle-skin interaction occurring at vesicle-skin interface (Fig. 4C-D). These variations (perturbation, cracks, roughness, inter-cellular spaces, and tiny fissures) are reversible and temporary after topical application for enhanced drug access across SC layer. Moreover, the surfactant is responsible for extracting lipid to disturb the lipid bilayer organized in the skin for improved vesicle permeation (Touitou et al., 2001). PC of the vesicles might have been self-assembled as lipid bilayer to get fused with the skin lipid for the vesicle's permeation. Highly lipophilic surfactants (span-80, HLB = 4.3) are known to extract lipid to cause reversible changes in corneocytes and interact with the skin protein. Thus, the composition of vesicles is the prime driving force deciding permeation profile of the drug loaded vesicles and maximized interaction with SC layer (3–10 column corneocytes) (Jun et al., 2013; Tzlein and Cevc, 1998). Moreover, vesicle characteristics such as; size, elasticity, surfaces charge density, nature and type of lipid, and hydration are significant factors to consider during formulation development for the expected permeation profile and the drug deposition to achieve therapeutic benefit. These variables are critical factors to control the technology transfer from laboratory to large-scale production. Highly elastic and small vesicles are easily squeezed into the inner region of epidermis across SC layer, which is a brick-and-mortar-like structure composed of corneocytes of hydrated keratin and non-polar lipid of the intercellular matrix. These vesicles permeate through combined mechanisms, including rapid aqueous phase evaporation, non-volatile organic content deposition after application on SC layer, established hydration gradient between SC layer and vesicle surface, and increased water content in the air exposed-SC layer and viable epidermis to develop a transepidermal hydration gradient. These mechanisms work in tandem, as explained before (Jun et al.,

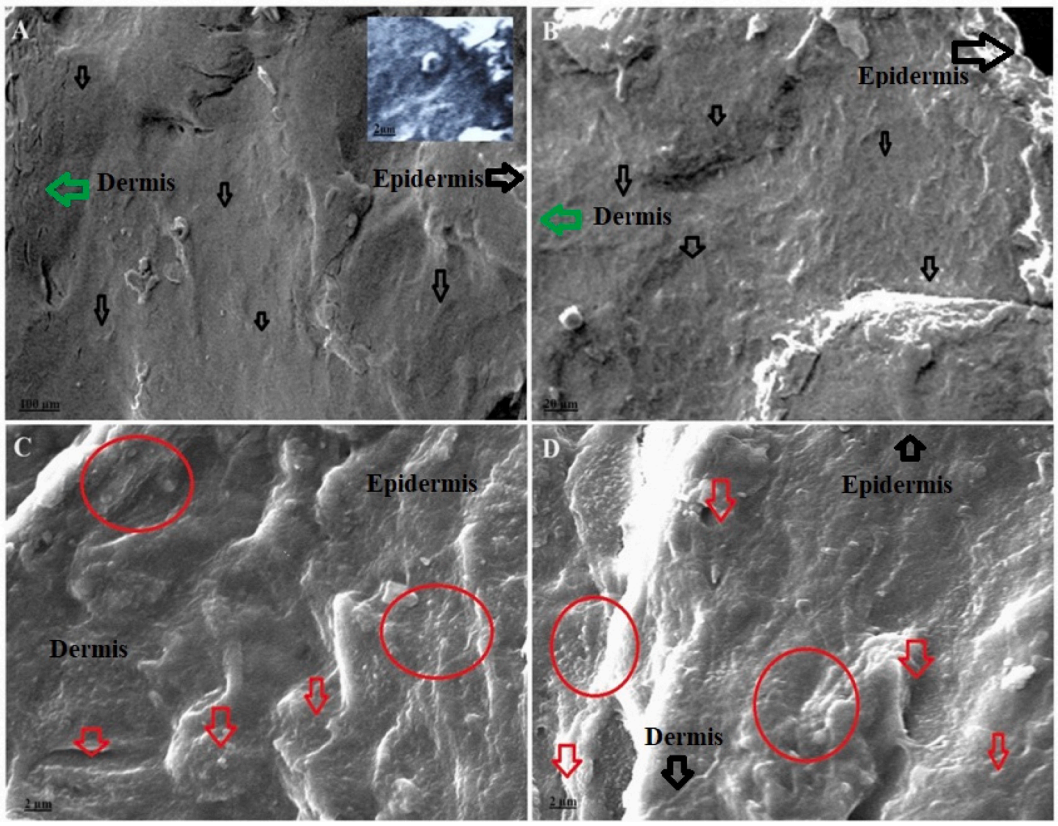

Fig. 4. Representative microphotographs of untreated (control) and treated rat skin under scanning electron microscopy: (A) the untreated control rat skin scanned at 100 µm exhibiting normal outer layer without perturbation (arrows indicated smooth skin surface without any surface perturbation) (magnification at 192×). Inset of A indicated untreated rat skin scanned at 2 µm elicited no significant perturbation, (B) DSR123 treated rat skin scanned at 20 µm revealing normal epidermis (arrows indicated intact surface morphology without crack, fissure, and perturbation) of SC (magnification at 1.97kX), (C) ODEL1-R123 caused substantial perturbation and reversible surface changes of SC layer (red arrows). Nanoscale vesicles are visible to interact with SC layer for amalgamation (lipid-lipid fusion) for permeation (as shown within encircled areas) (magnification at 1.97 kX), and (D) ODEL2-R123 caused the same degree of reversible perturbation as observed with ODEL1-R123 due to approximate composition and vesicle size (magnification at 1.97 kX and ETH = 15.00 kV). (For interpretation of the references to colour in this figure legend, the reader is referred to the web version of this article.)

2013; Tzlein and Cevc, 1998).

4.6. Mechanistic understanding of permeation

To understand mechanistic perspective of permeation, it is imperative to consider multiple aspects. The SEM allows for visualization of minute reversible or irreversible changes with high magnification. It provides extensive morphological information, aiding in understanding the mechanistic insight of the vesicle-skin interaction and the changes occurred. SEM technique was utilized to visualize the vesicles-skin interaction for the treated samples. As explored in our previous report for luteolin based elastic liposomes, the prime components - lipid (PC), span 80, and ethanol - rendered significant surface changes after topical application to rat skin (Altamimi et al., 2022; Utreja et al., 2011). These interactions involved H-bonding, lipid-lipid amalgamation, reversible bond breaking, polarity behavior of PC (lipid head) interacting with PO^{-2} polar head of skin lipid, London forces, and water mediated swelling by decreased transepidermal water loss for improved vesicle permeation across SC layer or through follicular drug access (Hansen and Andersen, 1998; Goh et al., 2022; Barry, 1987). Improved permeation may be attributed to the combined interactions working in tandem. A single interactive cannot be considered for augmented vesicle permeation across skin (specifically through intra-and intercellular pathways) (Goh et al., 2022; Lachenmeier, 2008). The permeation pathways are reversibly perturbed to make its ways for the vesicle transport towards inner dermal region as a result of aforementioned factors playing together. Thus, composition and formulation characteristics are prime critical quality attributes considered while developing transdermal delivery of desmopressin loaded elastic liposomes (Barry, 1987).

Different authors have reported two hydrophilic quantitative pathways with varied percentage of occurrence for permeation across SC layer. One is the inter-cluster route with low penetration resistance, and the second is the inter-corneocytes route as the most tortuous pathway (~ 80 % of pathway) (Jun et al., 2013; Tzlein and Cevc, 1998). Generally, the highly vascularized inner most dermis is relatively thicker (5–20 times) than epidermis (Jun et al., 2013; Tzlein and Cevc, 1998). Therefore, it is a prerequisite to optimize the vesicle characteristics and composition for maximized DA-loaded vesicles accessible to the dermal region for systemic availability. Therefore, the unique properties of elastic liposomes, which are ultra-deformable, high elasticity, and squeezable (through channels 1/10th the diameter of the ODEL1 vesicles), were exploited, optimized, and evaluated for transdermal delivery with high patient compliance. ODEL formulations are forcibly (by pull mechanism) permeated across SC layer under the developed gradient after non-occlusive application as gel (Cevc et al., 2008; Cevc and Vierl, 2010).

Physicochemical properties of basic ingredients of ODEL1 play profound role in enhancing transdermal flux and the drug deposition. Similarly, the critical characteristic properties of vesicles have a substantial impact on permeation profile. Therefore, the selection of lipid depends upon the desired glass transition temperature (T_m) to achieve optimal plasticity and fluidized nature of vesicle. An unsaturated lipid with $T_m < 0$ renders the fluid-chains vesicular lipid bilayer for improved skin permeation compared to conventional liposomes (Tzlein and Cevc, 1998). The edge activator is responsible for controlling elasticity and fluidity of lipid bilayer. Therefore, it was a prerequisite to optimize the concentration of edge activator to obtained desired size, drug entrapment, permeation flux, and ultra-deformability. Extreme high and low contents may cause unusual drug leakage and rigidity, respectively, after prolonged storage. Excess use of edge activator may predominantly form micelles than vesicles which can execute low sensitivity to water activity gradient in the skin (Cevc et al., 2003; Bekmukhametova et al., 2017; Zhiltsova et al., 2017). Considering above factors, highly lipophilic span 80 (HLB = 4.3) resulted in optimal vesicle size to load high drug content for maximized permeation/the drug deposition (Bnyan et al., 2018).

5. Conclusion

The presented finding provided continued insights into DA loaded elastic liposomes for mechanistic understanding of permeation process across SC of rat skin. The objective of HSP was to understand predictive interaction between the developed vesicles and skin surface. In general, normal human skin is related with δ_d, δ_p, and δ_H values of 12.0 (17.0), 8.0 (12), and 8.0 (11) $MPa^{1/2}$, respectively, which are close to the HSP values of ODEL1. The program predicted a strong interaction of ODEL1 vesicles with the skin surface. Therefore, it was further simulated with the instrumental based surface analysis, FTIR, DSC, and fluorescent microscopy. Interestingly, SEM and fluorescent microscopy studies confirmed substantial impact of the formulation composition and characteristics on surface perturbation for enhanced permeation and the drug deposition. FTIR confirmed variation in stretching and bond vibration as compared to the control group suggesting molecular interaction of the vesicle with surface protein of the skin. To confirm the changes in thermal behavior of the surface structure, DSC tool corroborated that vesicles triggered substantial variations (reversible) in the anatomical structure of protein layer resulting in high permeation and the drug deposition. All these strategic approaches concluded that ODEL1 exhibited maximized drug permeation through reversible and temporary changes generated in the skin surface for augmented permeation. This may be useful to understand mechanistic perspective of vesicle permeation maximize systemic availability of the drug. Moreover, a formulation scientist must have a basic understanding of material quality attributes and critical process parameters attributes for designing a robust transdermal product of desmopressin acetate delivery.

Ethical approval

The study was conducted according to the guidelines of the Declaration of Helsinki and approved (approved on 2nd December 2020) by the Institutional Review Board (or Ethics Committee) of College of Pharmacy, King Saud University (Institutional Animal House (Institutional ethical committee), Riyadh, Saudi Arabia (approved ethical No: KSU-SE-20-64). The protocol was followed as per ARRIVE guidelines. Rats were used when they attained age of around 5–6 months. Albino rats (weighing around 300 g) of either sex were used in the experiment as per the approved protocol.

Funding

Authors are thankful to the Researchers Supporting Project number (RSPD2024R524), King Saud University, Riyadh, Saudi Arabia, for supporting this work.

CRediT authorship contribution statement

Afzal Hussain: Writing – review & editing, Writing – original draft, Visualization, Validation, Software, Resources, Methodology, Investigation, Data curation, Conceptualization. **Mohammad A. Altamimi:** Project administration, Funding acquisition, Data curation. **Musaad A. Alshammari:** Visualization, Methodology, Investigation, Formal analysis, Data curation.

Declaration of competing interest

The authors report no conflict of interest.

Acknowledgement

The authors are thankful to the Researchers Supporting Project

number (RSPD2024R524), King Saud University, Riyadh, Saudi Arabia, for supporting this work.

Funding

The authors extend their appreciation to the Researchers Supporting Project number (RSPD2024R524), King Saud University, Riyadh, Saudi Arabia, for supporting this work.

Appendix A. Supplementary data

Supplementary data to this article can be found online at https://doi.org/10.1016/j.ijpx.2024.100304.

Data availability

Data will be made available on request.

References

Abbott, S., 2012. An integrated approach to optimizing skin delivery of cosmetic and pharmaceutical actives. Int. J. Cosmet. Sci. 34, 217–222.
Alam, Zeb, Qureshi, O.S., Kim, H.-S., Cha, J.-H., Kim, H.-S., Kim, J.-K., 2016. Improved skin permeation of methotrexate via nanosized ultradeformable liposomes. Int. J. Nanomedicine 11, 3813–3824.
Alkilani, A.Z., McCrudden, M.T.C., Donnelly, R.F., 2015. Transdermal drug delivery: innovative pharmaceutical developments based on disruption of the barrier properties of the stratum corneum. Pharmaceutics 7, 438–470.
Alshammari, M.A., Khan, M.R., Alasmari, F., Alshehri, A.O., Ali, R., Boudjelal, M., Alhosaini, K.A., Niazy, A.A., Alshammari, T.K., 2019. Changes in the fluorescence tracking of NaV1.6 protein expression in a BTBR T+Itpr3tf/J autistic mouse model. Neural Plasticity 1–12.
Altamimi, M.A., Hussain, A., Alshehri, S., Imam, S.S., 2021a. Experimental design based optimization and ex vivo permeation of desmopressin acetate loaded elastic liposomes using rat skin. Pharmaceutics 13 (7), 1047. https://doi.org/10.3390/pharmaceutics13071047.
Altamimi, M.A., Hussain, A., AlRajhi, M., Alshehri, S., Imam, S.S., Qamar, W., (2021b)b. Luteolin-loaded elastic liposomes for transdermal delivery to control breast cancer: in vitro and ex vivo evaluationsPharmaceuticals (Basel) 14(11), 1143. doi: https://doi.org/10.3390/ph14111143.
Altamimi, M.A., Hussain, A., Mahdi, W.A., Imam, S.S., Alshammari, M.A., Alshehri, S., Khan, M.R., 2022. Mechanistic insights into luteolin-loaded elastic liposomes for transdermal delivery: HSPiP predictive parameters and instrument-based evidence. ACS Omega 7 (51), 48202–48214.
Ananthapadmanabhan, K.P., Yu, K.K., Meyers, C.L., 1996. Aronson MP. Binding of surfactants to stratum corneum. J. Soc. Cosmet. Chem. 47, 185–200.
Barel, A.O., Paye, M., Maibach, H.I., 2009. Handbook of Cosmetic Science and Technology, 3rd ed. Marcel Dekker, New York, p. 2009.
Barry, B., 1987. Mode of action of penetration enhancers in human skin. J. Control. Release 6 (1), 85–97.
Bekmukhametova, A.M., Kashapov, R.R., Saifutdinova, M.N., Gavrilova, E.L., Mamedov, V.A., Zhukova, N.A., Zakharova, L.Y., Sinyashin, O.G., 2017. Aggregation and solubilization properties of system based on glycine-calix[4]resorcinol and sodium dodecyl sulfate in aqueous medium. Macroheterocycles 10 (2), 164–168.
Benson, H.A., 2006. Transfersomes for transdermal drug delivery. Expert Opin. Drug Deliv. 3 (6), 727–737.
Bnyan, R., Khan, I., Ehtezazi, T., Saleem, I., Gordon, S., Neill, F.O., 2018. Roberts M. Surfactant effects on lipid-based vesicles properties. J. Pharm. Sci. 107 (5), 1237–1246.
Cevc, G., Vierl, U., 2010. Nanotechnology and the transdermal route: a state of the art review and critical appraisal. J. Control. Release 141, 277–299.
Cevc, G., Schatzlein, A.G., Richardsen, H., Vierl, U., 2003. Overcoming semipermeable barriers, such as the skin, with ultradeformable mixed lipid vesicles, Transfersomes, liposomes or mixed lipid micelles. Langmuir 19, 10753–10763.
Cevc, G., Mazgareanu, S., Rother, M., Vierl, U., 2008. Occlusion effect on transcutaneous NSAID delivery from conventional and carrier-based formulations. Int. J. Pharm. 359, 190–197.
Christophers, E., Kligman, A.M., 1964. Visualization of the cell layers of the stratum corneum. J. Invest. Dermatol. 42, 407–409.
Cormier, M., Johnson, B., Ameri, M., Nyam, K., Libiran, L., Zhang, D.D., Daddona, P., 2004. Transdermal delivery of desmopressin using a coated microneedle array patch system. J. Control. Release 97 (3), 503–511.
Daisuke, N., Minoru, H., Riichiro, O., 2017. Nontoxic organic solvents identified using a Priori approach with Hansen solubility parameters. Chem. Commun. 53 (29), 4096–4099.
Dirscherl, K., Karlstetter, M., Ebert, S., Kraus, D., Hlawatsch, J., Walczak, Y., Moehle, C., Fuchshofer, R., Langmann, T., 2010. Luteolin triggers global changes in the microglial transcriptome leading to a unique anti-inflammatory and neuroprotective phenotype. J. Neuroinflammation 7, 1–16.
Dreher, F., Walde, P., Walther, P., Wehrli, E., 1997. Interaction of a lecithin microemulsion gel with human stratum corneum and its effect on transdermal transport. J. Control. Release 45 (2), 131–140.
Ezati, N., Robets, M.S., Zhang, Q., Moghimi, H.R., 2020. Measurement of Hansen Solubility Parameters of Human Stratum corneum. Iran. J. Pharm. Res. 19 (3), 572–578.
Godin, B., Touitou, E., 2007. Transdermal skin delivery: Prediction for humans from in vitro, ex vivo, and animal models. Adv. Drug Deliv. Rev. 59 (11), 1152–1161.
Goh, C.F., Hadgraft, J., Lane, M.E., 2022. Thermal analysis of mammalian stratum corneum using differential scanning calorimetry for advancing skin research and drug delivery. Int. J. Pharm. 614, 121447. https://doi.org/10.1016/j.ijpharm.2021.121447.
Hansen, C.M., 2007. Hansen Solubility Parameters: A User's Handbook, Second Edition (2nd ed.). CRC Press, pp. 1–544. https://doi.org/10.1201/9781420006834.
Hansen, C.M., Andersen, B.H., 1998. The affinities of organic solvents in biological systems. Am. Ind. Hyg. Assoc. J. 49 (6), 301–308.
Hosseini, M., Roberts, M.S., Aboofazeli, R., Moghimi, H.R., 2021. Measurement of Hansen Solubility Parameters of third degree burn eschar. Burns 21, 202–203.
Hossin, B., Rizi, K., Murdan, S., 2016. Application of Hansen Solubility Parameters to predict drug-nail interactions, which can assist the design of nail medicines. Eur. J. Pharm. Biopharm. 102, 32–40.
Hussain, A., Samad, A., Singh, S.K., Ahsan, M.N., Haque, M.W., Faruk, A., Ahmed, F.J., 2016. Nanoemulsion gel-based topical delivery of an antifungal drug: in vitro activity and in vivo evaluation. Drug Deliv. 23 (2), 642–657.
Hussain, A., Singh, S., Sharma, D., Webster, T.J., Shafaat, K., Faruk, A., 2017. Elastic liposomes as novel carriers: recent advances in drug delivery. Int. J. Nanomedicine 12, 5087–5108.
Hussain, A., Altamimi, M.A., Alshehri, S., Imam, S.S., Singh, S.K., 2020. Vesicular elastic liposomes for transdermal delivery of rifampicin: In-vitro, in-vivo and in silico GastroPlus™ prediction studies. Eur. J. Pharm. Sci. 105411. https://doi.org/10.1016/j.ejps.2020.105411.
Jain, S., Tiwary, A.K., Sapra, B., Jain, N.K., 2007. Formulation and evaluation of ethosomes for transdermal delivery of lamivudine. AAPS PharmSciTech 8 (4), 249–257.
Jun, C., Wen-Li, L., Wei, G., Shan-Shan, L., Zhi-Peng, C., Bao-Chang, C., 2013. Skin permeation behavior of elastic liposomes: role of formulation ingredients. Expert Opin. Drug Deliv. 10 (6), 845–856.
Kalita, B., Das, M.K., 2018. Rutin–phospholipid complex in polymer matrix for long-term delivery of rutin via skin for the treatment of inflammatory diseases. Art. Cells Nanomed. Biotechnol. 46, 41–56.
Khan, T., Hussain, A., Siddique, M.U.M., Altamimi, M.A., Malik, A., Bhat, Z.R., 2024. HSPiP, computational, and thermodynamic model-based optimized solvents for subcutaneous delivery of tolterodine tartrate and GastroPlus-based in vivo prediction in humans: Part II. AAPS PharmSciTech 25 (6), 160. https://doi.org/10.1208/s12249-024-02880-0.
Kirjavainen, M., Urtti, A., Jääskeläinen, I., Suhonen, T.M., Paronen, P., Valjakka-Koskela, R., Kiesvaara, J., Mönkkönen, J., 1996. Interaction of liposomes with human skin in vitro — the influence of lipid composition and structure. Biochim. Biophys. Acta 1304 (3), 1–189.
Kyounghee, S., Hayoung, C., Kwang, S.S., Won, Y.J., Yong, L.J., Ji, C.E., Hee, L.D., Hee, D.S., Woong, K.J., 2018. Nanoemulsion vehicles as carriers for follicular delivery of luteolin. ACS Biomater. Sci. Eng. 8b00220. https://doi.org/10.1021/acsbiomaterials.8b00220.
Lachenmeier, D.W., 2008. Safety evaluation of topical applications of ethanol on the skin and inside the oral cavity. J. Occup. Med. Toxicol. 3 (1), 26. https://doi.org/10.1186/1745-6673-3-26.
Lei, F., Zhang, H., Luo, R., Fei, Q., Bai, L., He, N., 2022. Sustained ocular delivery of desmopressin acetate via thermoreversible in situ gel formulation: preparation and in vitro/in vivo evaluation. J. Pharm. Investig. 52, 639–648.
Lin, Y., Shi, R., Wang, X., Shen, H.-M., 2008. Luteolin, a flavonoid with potential for cancer prevention and therapy. Curr. Cancer Drug Targets 8, 634–646.
Mirgorodskaya, A.B., Mamedov, V.A., Zakharova, L.Y., Valeeva, F.G., Mamedova, V.L., Galimullina, V.R., Kushnasarova, R.A., Sinyashin, O.G., 2017. Surfactant solutions for enhancing solubility of new arylquinolin-2-ones. J. Mol. Liq. 242, 732–738.
Ahmed, O.A., Rizq, W.Y., 2018. Finasteride nano-transferosomal gel formula for management of androgenetic alopecia: ex vivo investigational approach. Drug Des. Devel. Ther. 12, 2259–2265.
Pal, A., Sunthar, P., Khakhar, D.V., 2019. Effects of ethanol addition on the size distribution of liposome suspensions in water. Eng. Chem. Res. 58, 7511–7519.
Parker, F.S., 1993. Application of infrared spectroscopy in biochemistry, biology, and medicine. Plenum, 1971, New York, United States of America. In: Diem, M. (Ed.), Introduction to Modern Vibrational Spectroscopy. Wiley–Interscience, New York, USA, 1993.
Perkins, W.R., Minchey, S.R., Ahl, P.L., Janoff, A.S., 1993. The determination of liposome captured. Chem. Phys. Lipids 64 (1–3), 197–217.
Pilch, E., Musiał, W., 2018. Liposomes with an ethanol fraction as an application for drug delivery. Int. J. Mol. Sci. 19 (12), 3806. https://doi.org/10.3390/ijms19123806.
Ramzan, M., Khan, T., Siddique, M.U.M., Shahid, M., 2024. Biocompatible cationic 5-fluorouracil loaded elastic liposomes for ocular delivery: in vitro, ex vivo, and in vivo evaluation. J. Drug Deliv. Sci. Technol. 101 (Part B), 106278.
Salimi, A., Hedayatipour, N., Moghimipour, E., 2016. The effect of various vehicles on the naproxen permeability through rat skin: a mechanistic study by DSC and FT-IR techniques. Adv. Pharm. Bull. 6 (1), 9–16.
Scheuplein, R.J., 1967. Mechanisms of percutaneous absorption. II. Transient diffusion and the relative importance of various routes of skin penetration. J. Invest. Dermatol. 48 (1), 79–88.

Souto, E.B., Macedo, A.S., Dias-Ferreira, J., Cano, A., Zielińska, A., Matos, C.M., 2021. Elastic and ultradeformable liposomes for transdermal delivery of active pharmaceutical ingredients (APIs). Int. J. Mol. Sci. 22 (18), 9743. https://doi.org/10.3390/ijms22189743.

Touitou, E., Godin, B., Dayan, N., Weiss, C., Piliponsky, A., Levi-Schaffer, F., 2001. Intracellular delivery mediated by an ethosomal carrier. Biomaterials 22, 3053–3059.

Tzlein, A.C., Cevc, G., 1998. Non-uniform cellular packing of the stratum corneum and permeability barrier function of intact skin: a high-resolution confocal laser scanning microscopy study using highly deformable vesicles (Transfersomes). Br. J. Dermatol. 138, 583–592.

Utreja, P., Jain, S., Tiwary, A.K., 2011. Localized delivery of paclitaxel using elastic liposomes: Formulation development and evaluation. Drug Deliv. 18 (5), 367–376.

Wu, G., Li, J., Yue, J., Zhang, S., Yunusi, K., 2018. Liposome encapsulated luteolin showed enhanced antitumor efficacy to colorectal carcinoma. Mol. Med. Rep. 17, 2456–2464.

Zhiltsova, E.P., Ibatullina, M.R., Lukashenko, S.S., Valeeva, F.G., Pashirova, T.N., Kutyreva, M.P., Zakharova, L.Y., 2017. Complexes of 1-hexadecyl-4-aza-1-azonia-bicyclo[2.2.2]octane bromide with transition metal nitrates. Micelle-forming, solubilizing, and adsorption properties. Colloid J. 79 (5), 621–629.